Microfluid Nanofluid
DOI 10.1007/s10404-010-0564-9

RESEARCH PAPER

# Rarefied gas flow of binary mixtures through long channels with triangular and trapezoidal cross sections

**Lajos Szalmas · Dimitris Valougeorgis**

Received: 16 October 2009 / Accepted: 15 December 2009


**Abstract** The flow of binary gas mixtures through long micro-channels with triangular and trapezoidal cross sections is investigated in the whole range of the Knudsen number. The flow is driven by pressure and concentration gradients. The McCormack kinetic model is utilized to simulate the rarefied flow of the gas mixture, and the kinetic equations are solved by an upgraded discrete velocity algorithm. The kinetic dimensionless flow rates are tabulated for selected noble gas mixtures flowing through micro-channels etched by KOH in silicon (triangular and trapezoidal channels with acute angle of 54.74°). Furthermore, the complete procedure to obtain the mass flow rate for a gas mixture flowing through a channel, based on the dimensionless kinetic results, which are valid in each cross section of the channel, is presented. The study includes the effect of the separation phenomenon. It is shown that gas separation may change significantly the estimated mass flow rate. The presented methodology can be used for engineering purposes and for the accurate comparison with experimental results.

**Keywords** Rarefied gas flows · Binary mixtures · Gas separation · Discrete velocity method

## 1 Introduction

The non-equilibrium gas flow through channels of various cross sections has recently attracted considerable attention. This increased interest is well justified by the implementation of such flows in several technological fields including the emerging field of microfluidics (Ho and Tai 1998; Karniadakis and Beskok 2002; Kandlikar et al. 2006; Li 2008).

The majority of the research has been performed for flows through circular and rectangular micro-channels, where both theoretical and experimental studies have been implemented. The theoretical study has been based on hydrodynamics beyond the Navier–Stokes limit (Colin 2005; Lockerby and Reese 2008; Szalmas 2007), the Direct Simulation Monte Carlo method (Bird 1994), and kinetic theory as described by the Boltzmann and model kinetic equations (Ferziger and Kaper 1972; Cercignani 1988). It is important to note that for flows through long channels, where the flow may be considered as fully developed, linearized kinetic theory is overall, the most powerful theoretical approach, since it is capable of producing accurate results in the whole range of the Knudsen number with modest computational effort (Aoki 2001; Sharipov 1999). Experimental study in long micro-channels is also very extensive, and the most common experimental approaches include the constant volume and the droplet tracking methods (Colin et al. 2004; Ewart et al. 2007).

Flows through long channels of other cross sections have also been studied. In particular, rarefied gas flow through long tubes with elliptical cross section has been recently solved by using linearized kinetic models (Graur and Sharipov 2007, 2008). The linearized BGK model has been also solved for annular tubes (Breyiannis et al. 2008). Based on Navier–Stokes solvers, with slip boundary conditions, the pressure-driven flow through channels of triangular and trapezoidal cross sections in the slip regime has been solved (Morini et al. 2004, 2005; Pitakarrnop et al. 2008). Also, in more recent studies, the same flow configuration has been solved in the whole range of the Knudsen number by using the linearized BGK kinetic

L. Szalmas (✉) · D. Valougeorgis
Department of Mechanical and Industrial Engineering, University of Thessaly, Pedion Areos, Volos 38334, Greece
e-mail: lszalmas@gmail.com

Published online: 21 January 2010

model (Naris and Valougeorgis 2008; Varoutis et al. 2009). In Varoutis et al. (2009), a comparison between computational and experimental results has been performed finding, in all the cases, very good agreement. It is noted that channels with triangular and trapezoidal cross sections, with an acute angle of 54.74°, manufactured by chemical etching on silicon wafers, known as microchannels etched by KOH in silicon, are very common in microflow applications (Morini et al. 2004, 2005).

The majority of all this research study has been performed for single gases, while the corresponding study for gaseous mixtures is quite limited. In the latter case, the McCormack kinetic model (McCormack 1973) has been applied for flows of binary mixtures through channels of circular and rectangular cross sections (Sharipov and Kalempa 2002; Naris et al. 2005). In addition to flows through channels, the McCormack model has been solved for Couette flow (Sharipov et al. 2004) or heat flow between two parallel plates (Sharipov et al. 2007). The analytical discrete ordinate method has been also used to solve various one-dimensional flow problems on the basis of the McCormack kinetic model (Siewert and Valougeorgis 2004a, b). A first attempt to measure pressure-driven mass flow rates for binary mixtures through rectangular channels is reported in Pitakarnnop (2010). The small amount of study in the case of gas mixture flows may be explained by the increased complexity of the flow due to the large number of parameters involved in the solution of the problem. However, gaseous mixture, compared to single gas flows, have increased theoretical and practical interest. In the case of gas mixtures, additional non-equilibrium transport phenomena (e.g., barodiffusion) appear, as the rarefaction of the flow is increased. Also, in microfluidic applications, the flow in most cases consists of gas mixtures and not of single gases. Another important transport phenomenon of great practical interest appearing in flows of gas mixtures is the separation phenomenon. The light particles are traveling faster than the heavier ones resulting to the change of the concentration of the gas mixture as it flows along the channel. This situation, known as the separation effect, must be taken into account in simulations and may be useful in the design of gaseous microsystems (Sharipov and Kalempa 2005; Takata et al. 2007; Sugimoto 2009).

In this article, a fully developed binary rarefied gas flow through long triangular and trapezoid channels is investigated. Pressure- and concentration-driven microflows are considered. The flow is modeled by the McCormack kinetic model subject to Maxwell diffuse-specular boundary conditions. The kinetic integro-differential equations are solved in a very efficient manner, and the obtained results are valid in the whole range of the rarefaction from the free molecular through the transition up to the hydrodynamic limit. Numerical results are presented for the noble-gas mixtures of *Ne*/*Ar* and *He*/*Xe*. Even more, a detailed procedure is presented for calculating the mass flow rate from the dimensionless kinetic coefficients taking into account the separation phenomenon. The presented methodology and results can be used for comparing experiments with theory, as well as to the design and optimization of micro devices.

## 2 Flow configuration

Consider the isothermal flow of a gaseous mixture through a channel of length $L$, with triangular or trapezoidal cross sections. The cross sections are defined by the $x'$ and $y'$ coordinates, while the flow is assumed to be in the direction of the $z'$ coordinate. The perimeter and the area of the channel are denoted by $\Gamma'$ and $A'$, respectively. The hydrodynamic diameter of the channel $D_h = 4A'/\Gamma'$ is utilized as the characteristic length of the problem. End effects are ignored by taking $D_h << L$.

The dimensionless spatial variables $x = x'/D_h$, $y = y'/D_h$, and $z = z'/D_h$ are introduced, while the dimensionless perimeter and area are defined as $\Gamma = \Gamma'/D_h$ and $A = A'/D_h^2$, respectively. The cross sections are presented in Fig. 1. It is noted that the dimensionless geometry of the trapezoidal cross section is completely characterized by the acute angle $\omega$ and the ratio of the small base $b$ to the height $h$. The triangular channel is recovered from the trapezoidal one by taking $b/h = 0$. The dimensionless coordinates of the vertexes of the trapeze $(x, y)$ on the large base are given by $(\pm B/(2D_h), 0)$, while on the small base by $(\pm b/(2D_h), h/D_h)$. The explicit expressions of the dimensionless coordinates to define the computational domain, in terms of $\omega$ and $b/h$ are:

$$\frac{h}{D_h} = \frac{1}{2}\frac{b/h + 1/\tan\omega + 1/\sin\omega}{b/h + 1/\tan\omega} \tag{1}$$

$$\frac{b}{2D_h} = \frac{1}{4}(b/h)\frac{b/h + 1/\tan\omega + 1/\sin\omega}{b/h + 1/\tan\omega} \tag{2}$$

$$\frac{B}{2D_h} = \frac{1}{4}(b/h + 2/\tan\omega)\frac{b/h + 1/\tan\omega + 1/\sin\omega}{b/h + 1/\tan\omega} \tag{3}$$

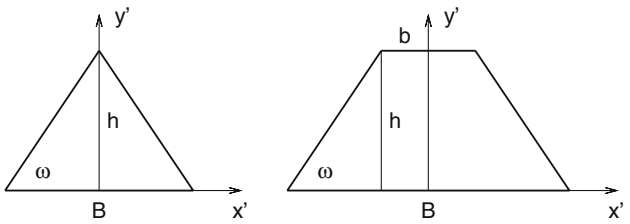


**Fig. 1** The cross sections of the isosceles triangular and trapezoidal channels

By setting in Eqs. 1 and 3, $b/h = 0$, the dimensionless coordinates of the isosceles triangular are deduced.

The mixture consists of two components. The molecular masses and the number densities of the two species are denoted by $m_\alpha$ and $n_\alpha$ for components $\alpha = 1, 2$. In this study, without loss of generality, $m_1$ will always refer to the light species of the mixture. The average molecular mass of the mixture is defined by

$$m(C) = Cm_1 + (1 - C)m_2, \tag{4}$$

where

$$C = \frac{n_1}{n_1 + n_2}, \tag{5}$$

is the concentration of the light species in the mixture. The total number density of the mixture is obtained by $n = n_1 + n_2$. Other important quantities of the mixture, for the purposes of this study, are its viscosity $\mu(C)$ and its characteristic molecular velocity $v(C) = \sqrt{2kT/m(C)}$, with $k$ denoting the Boltzmann constant and $T$ the temperature of the flow. Since this is an isothermal flow, both quantities depend only on the concentration of the mixture.

The flow is maintained by a pressure and/or concentration gradient defined by

$$X_P = \frac{D_h}{P}\frac{\partial P}{\partial z'} = \frac{1}{P}\frac{\partial P}{\partial z} \tag{6}$$

and

$$X_C = \frac{D_h}{C}\frac{\partial C}{\partial z'} = \frac{1}{C}\frac{\partial C}{\partial z} \tag{7}$$

respectively. Here, $P = P(z)$ and $C = C(z)$ are the pressure and concentration distributions along the channel and, in general, their gradients are not constant. It is important to note that under the assumption of $D_h << L$ both the dimensionless gradients are always much less than one, i.e., $|X_P| << 1$, $|X_C| << 1$, independently of the magnitude of the pressure and concentration differences between the inlet and the outlet of the channel.

The flow is characterized by the rarefaction parameter defined by

$$\delta = \frac{D_h P(z)}{\mu(C)v(C)}, \tag{8}$$

It is emphasized that the rarefaction parameter varies in the flow direction, i.e., $\delta = \delta(z)$, according to the variation of the pressure, viscosity, and characteristic velocity along the channel. The rarefaction parameter is proportional to the inverse Knudsen number.

Under the assumption of the long channel (fully developed flow) the only non-zero component of the macroscopic (bulk) velocity vectors $\boldsymbol{u}'_\alpha$ of the two species is the $z'$ component, which is the function of the transverse coordinates, i.e., $\boldsymbol{u}'_\alpha = (0, 0, u'_\alpha(x', y'))$, with $\alpha = 1, 2$. Other relevant macroscopic quantities concerning the flow problem are the heat flow vectors having non-zero element only for the $z'$ component $\boldsymbol{q}'_\alpha = (0, 0, q'_\alpha(x', y'))$ and the traceless pressure tensors having non-zero elements only for $p'_{\alpha xz}(x', y'), p'_{\alpha yz}(x', y')$, with $\alpha = 1, 2$.

In addition to the bulk velocity of the two species, we are introducing the mean velocity of the mixture as

$$w(x', y') = \frac{n_1 u'_1 + n_2 u'_2}{n_1 + n_2}. \tag{9}$$

We are interested in the overall quantities of the mass flow rate given by

$$\dot{M} = \iint_{A'} (n_1 m_1 u'_1 + n_2 m_2 u'_2) dx' dy' \tag{10}$$

and of the particle and concentration fluxes defined by (Sharipov and Kalempa 2002; Naris et al. 2005)

$$J_P = -n \iint_{A'} w dx' dy', \tag{11}$$

$$J_C = -n_1 \iint_{A'} (u'_1 - u'_2) dx' dy'. \tag{12}$$

It is readily seen that these overall quantities are interconnected by the expression

$$\dot{M} = -m(C)J_P + (m_2 - m_1)(1 - C)J_C. \tag{13}$$

The particle and concentration fluxes are connected to the gradients of the pressure and the concentration via the dimensionless kinetic coefficients, namely, $\Lambda_{PP}$, $\Lambda_{CP}$, $\Lambda_{PC}$, $\Lambda_{CC}$ in the following way:

$$J_P = \frac{nA'v(C)}{2}[\Lambda_{PP}X_P + \Lambda_{PC}X_C], \tag{14}$$

$$J_C = \frac{nA'v(C)}{2}[\Lambda_{CP}X_P + \Lambda_{CC}X_C]. \tag{15}$$

It is noted that the $J_P$ and $J_C$ fluxes are two independent variables since $J_P$ describes the total particle flow rate, while $J_C$ is related to the velocity difference between the components. The driving terms, $X_P$ and $X_C$, are also independent quantities. $X_P$ is related to the total number density, while $X_C$ to the ratio of the component densities. The use of the $X_P$, $X_C$ driving terms are straightforward and advantageous since the pressure and the concentration are the two main quantities in the description of gaseous mixtures and the related micro-gas flow applications.

The cross kinetic coefficients are not independent, and they are connected via the Onsager–Casimir relationship $\Lambda_{PC} = \Lambda_{CP}$, as it was shown in Sharipov (1994).

The rarefied gas flow in the channel is completely characterized by the above mentioned kinetic coefficients. It is important to emphasize that these are local quantities and

describe the flow in a given cross section with the corresponding $X_P$ and $X_C$ gradients. In this article, our goal is to calculate and tabulate the kinetic coefficients for different values of $\delta$ and $C$ and then, based on these kinetic results, to provide the detailed procedure for estimating the overall mass flow rate, taking into account the pressure and concentration variation along the channel including the separation effect.

## 3 Kinetic description

In order to simulate the flow, a kinetic description, based on the McCormack model subject to the Maxwell diffuse-specular boundary conditions is adapted. The approach is valid in the whole range of the rarefaction.

The basic quantity in the description of the problem is the distribution function $f_\alpha(\boldsymbol{c}_\alpha, x, y, z)$ for components $\alpha = 1, 2$. Here, $\boldsymbol{c}_\alpha = (c_{\alpha x}, c_{\alpha y}, c_{\alpha z})$ is the dimensionless molecular velocity defined by $\boldsymbol{c}_\alpha = \boldsymbol{v}_\alpha (m_\alpha/2kT)^{1/2}$ with $\boldsymbol{v}_\alpha$ being the molecular velocity. The distribution function is linearized such that

$$f_\alpha(\boldsymbol{c}_\alpha, x, y, z) = f_\alpha^{(0)}(\boldsymbol{c}_\alpha, z)(1 + h_\alpha(\boldsymbol{c}_\alpha, x, y)), \tag{16}$$

where $h_\alpha(\boldsymbol{c}_\alpha, x, y)$ is the perturbation function and $f_\alpha^{(0)}(\mathbf{c}_\alpha, z)$ is the equilibrium distribution

$$f_\alpha^{(0)}(\boldsymbol{c}_\alpha, z) = n_\alpha(z)\left(\frac{m_\alpha}{2\pi kT}\right)^{-3/2} e^{-c_\alpha^2}. \tag{17}$$

The perturbation function obeys the McCormack kinetic model

$$c_{\alpha x}\frac{\partial h_\alpha}{\partial x} + c_{\alpha y}\frac{\partial h_\alpha}{\partial y} = \omega_\alpha \sum_{\beta=1}^{2} L_{\alpha\beta} h_\alpha - c_{\alpha z}[X_P + \eta_\alpha X_C], \tag{18}$$

where $L_{\alpha\beta}$ is the McCormack collision term, which, together with $\omega_\alpha$, are defined in Appendix 1. In addition, the quantity $\eta_\alpha$ is given by

$$\eta_1 = 1, \quad \eta_2 = -\frac{C}{1-C}. \tag{19}$$

The non-dimensional velocity, heat flow, and traceless pressure tensor are obtained as the moments of the perturbation function:

$$\begin{aligned} u_\alpha &= \pi^{-3/2}\left(\frac{m}{m_\alpha}\right)^{1/2} \int_{-\infty}^{\infty} h_\alpha c_{\alpha z} e^{-c_\alpha^2} d\mathbf{c}_\alpha, \\ q_\alpha &= \pi^{-3/2}\left(\frac{m}{m_\alpha}\right)^{1/2} \int_{-\infty}^{\infty} h_\alpha c_{\alpha z}\left(c_\alpha^2 - \frac{5}{2}\right) e^{-c_\alpha^2} d\mathbf{c}_\alpha, \\ p_{\alpha i z} &= \pi^{-3/2} \int_{-\infty}^{\infty} h_\alpha c_{\alpha i} c_{\alpha z} e^{-c_\alpha^2} d\mathbf{c}_\alpha. \end{aligned} \tag{20}$$

In this formulation, the index $i$ refers to the coordinates $x$ or $y$.

In the present flow configuration, the problem can be described by the following two reduced distribution functions:

$$\Phi_\alpha = \frac{1}{\sqrt{\pi}}\sqrt{\frac{m}{m_\alpha}} \int_{-\infty}^{\infty}\int_{-\infty}^{\infty} h_\alpha c_{\alpha z} e^{-c_\alpha^2 - c_\alpha^2} dc_{\alpha z}, \tag{21}$$

$$\Psi_\alpha = \frac{1}{\sqrt{\pi}}\sqrt{\frac{m}{m_\alpha}} \int_{-\infty}^{\infty}\int_{-\infty}^{\infty} h_\alpha c_{\alpha z}^3 e^{-c_\alpha^2 - c_\alpha^2} dc_{\alpha z}. \tag{22}$$

In accordance with the McCormack model, Eq. 18, the reduced distribution functions obey the following system of four linear integro-differential equations:

$$\begin{aligned} c_{\alpha x}\frac{\partial \Phi_\alpha}{\partial x} + c_{\alpha y}\frac{\partial \Phi_\alpha}{\partial y} + \gamma_\alpha \omega_\alpha \Phi_\alpha &= -\frac{1}{2}\sqrt{\frac{m}{m_\alpha}}[X_P + \eta_\alpha X_C] \\ &+ \omega_\alpha \sum_{\beta=1}^{2}\Big[A_{\alpha\beta} + 2B_{\alpha\beta x} c_{\alpha x} + 2B_{\alpha\beta y} c_{\alpha y} \\ &+ \frac{2}{5} C_{\alpha\beta}(c_{\alpha x}^2 + c_{\alpha y}^2 - 1)\Big] \end{aligned} \tag{23}$$

and

$$\begin{aligned} c_{\alpha x}\frac{\partial \Psi_\alpha}{\partial x} + c_{\alpha y}\frac{\partial \Psi_\alpha}{\partial y} + \gamma_\alpha \omega_\alpha \Psi_\alpha &= -\frac{3}{4}\sqrt{\frac{m}{m_\alpha}}[X_P + \eta_\alpha X_C] \\ &+ \omega_\alpha \sum_{\beta=1}^{2}\Big[\frac{3}{2}A_{\alpha\beta} + 3B_{\alpha\beta x} c_{\alpha x} + 3B_{\alpha\beta y} c_{\alpha y} \\ &+ \frac{3}{5} C_{\alpha\beta}\left(c_{\alpha x}^2 + c_{\alpha y}^2\right)\Big], \end{aligned} \tag{24}$$

with $\alpha = 1, 2$.

The coefficients $A_{\alpha\beta}$, $B_{\alpha\beta i}$ and $C_{\alpha\beta}$ are connected to the bulk quantities of velocity $u_\alpha$, heatflow $q_\alpha$, and pressure $p_{\alpha i z}$ such that

$$A_{\alpha\beta} = \gamma_{\alpha\beta} u_\alpha - \nu_{\alpha\beta}^{(1)}(u_\alpha - u_\beta) - \frac{1}{2}\nu_{\alpha\beta}^{(2)}\left(q_\alpha - \frac{m_\alpha}{m_\beta} q_\beta\right), \tag{25}$$

$$B_{\alpha\beta i} = \left(\gamma_{\alpha\beta} - \nu_{\alpha\beta}^{(3)}\right)\sqrt{\frac{m}{m_\alpha}} p_{\alpha i z} + \nu_{\alpha\beta}^{(4)}\sqrt{\frac{m}{m_\alpha}} p_{\beta i z}, \tag{26}$$

$$C_{\alpha\beta} = \left(\gamma_{\alpha\beta} - \nu_{\alpha\beta}^{(5)}\right) q_\alpha + \nu_{\alpha\beta}^{(6)}\sqrt{\frac{m_\beta}{m_\alpha}} q_\beta - \frac{5}{4}\nu_{\alpha\beta}^{(2)}(u_\alpha - u_\beta). \tag{27}$$

The parameters $\gamma_{\alpha\beta}$ and $\nu_{\alpha\beta}$ are presented in Appendix 1.

Utilizing the reduced distribution functions, the bulk quantities are obtained by

$$u_\alpha = \frac{1}{\pi}\int_{-\infty}^{\infty}\int_{-\infty}^{\infty} \Phi_\alpha e^{-c_{\alpha x}^2 - c_{\alpha y}^2} dc_{\alpha x} dc_{\alpha y}, \tag{28}$$

$$q_\alpha = \frac{1}{\pi}\int_{-\infty}^{\infty}\int_{-\infty}^{\infty}\left[\Psi_\alpha + \left(c_{\alpha x}^2 + c_{\alpha y}^2 - \frac{5}{2}\right)\Phi_\alpha\right] e^{-c_{\alpha x}^2 - c_{\alpha y}^2} dc_{\alpha x} dc_{\alpha y}, \tag{29}$$

$$p_{\alpha iz} = \frac{1}{\pi}\sqrt{\frac{m}{m_\alpha}}\int_{-\infty}^{\infty}\int_{-\infty}^{\infty} c_{\alpha i}\Phi_\alpha e^{-c_{\alpha x}^2 - c_{\alpha y}^2} dc_{\alpha x} dc_{\alpha y}. \tag{30}$$

For the reduced distribution functions, the boundary conditions are written by

$$\Phi^+ = (1-\sigma)\Phi^-, \quad \Psi^+ = (1-\sigma)\Psi^-, \tag{31}$$

where $0 \le \sigma \le 1$ is the accommodation coefficient, while the $+$ and $-$ superscripts denote distributions representing particles departing from and arriving to the walls, respectively.

The above system of kinetic Eqs. 23 and 24 with the associated moments (28–30), subject to boundary conditions (31), has been solved numerically by discretizing in the physical space using a finite difference scheme on a boundary fitted triangular grid and in the molecular velocity space the discrete velocity method. The discretized equations are solved in an iterative manner. This numerical scheme has been extensively used in the past and for further details, the interested reader may refer to Naris and Valougeorgis (2008), Sharipov and Kalempa (2002), and Naris et al. (2005). The triangular grid is structured and consists of identical triangular elements (Naris and Valougeorgis 2008). In addition, in this study, in order to make the overall computation more efficient, a diffusion-type acceleration scheme is used to speed up the slow convergence of the algorithm in the nearly continuum region. The diffusion equations of the accelerated method are presented in Appendix 2.

Once the solution of the integro-differential system is obtained, the dimensionless flow rates of the components are deduced as

$$G_\alpha = -\frac{2}{A}\iint_A u_\alpha dxdy, \quad \alpha = 1, 2. \tag{32}$$

It is noted that the above described kinetic problem is linear, and, as a consequence, the solution may be decomposed in terms of $X_P$ and $X_C$. This is also the case for the dimensionless flow rate, which can be decomposed by

$$G_\alpha = G_\alpha^{(P)} X_P + G_\alpha^{(C)} X_C. \tag{33}$$

Then, for a pressure-driven flow, the kinetic coefficients $\Lambda_{PP}$ and $\Lambda_{CP}$ are calculated from

$$\Lambda_{PP} = CG_1^{(P)} + (1-C)G_2^{(P)}, \quad \Lambda_{CP} = C\left(G_1^{(P)} - G_2^{(P)}\right), \tag{34}$$

while for a concentration-driven flow, the kinetic coefficients $\Lambda_{PC}$ and $\Lambda_{CC}$ are calculated from

$$\Lambda_{PC} = CG_1^{(C)} + (1-C)G_2^{(C)}, \quad \Lambda_{CC} = C(G_1^{(C)} - G_2^{(C)}). \tag{35}$$

In Sect. 6.1, tabulated results are presented for the kinetic coefficients of two typical binary gas mixtures in terms of $\delta$ and $C$, flowing through one triangular and two trapezoidal channels.

## 4 Mass flow rate of gaseous mixture flowing through a channel

In applications, the mass flow rate $\dot{M}$, defined by Eq. 10, of a gaseous mixture flowing through a channel, connecting two reservoirs, is a very important quantity. Utilizing the kinetic coefficients, the mass flow rate can be calculated for realistic situations, provided that the pressure and the concentration of the upstream and downstream reservoirs, denoted by $I$ and $II$, respectively, as well as the geometry of the channel are known. In this section, the detailed methodology for deducing $\dot{M}$ is presented for flow caused by either a pressure or a concentration gradient. This section provides an approximation for the mass flow rate with the assumption that the concentration (or the pressure) is constant for the pressure (or concentration-)-driven flow. The analysis is valid for any pressure or concentration differences between the reservoirs as long as the restriction $D_h/L << 1$ holds.

### 4.1 Pressure-driven flow

In this case, the flow is maintained by a constant pressure drop between the containers. The pressures in the upstream and downstream reservoirs are given by $P_I$ and $P_{II}$, respectively, while the concentration in the containers and along the channels is considered constant and equal to $C_0$. Substituting Eqs. 14 and 15 for the $J_P$ and $J_C$ fluxes, with $X_C = 0$, into Eq. 13 and utilizing the ideal gas law $P = nkT$, as well as the definition of the characteristic velocity, the mass flow rate can be written as

$$\dot{M} = \left[-\Lambda_{PP} + \frac{m_2 - m_1}{m(C_0)}(1-C_0)\Lambda_{CP}\right]\frac{A'}{\nu(C_0)}\frac{dP}{dz}. \tag{36}$$

It is important to note that in Eq. 36, the mass flow rate is given in terms of quantities which vary along the channel and refer to a given cross section. Of course, the mass flow rate is a quantity, which, due to mass conservation, is constant at each cross section. Then, the mass flow rate may be also

defined in terms of reference quantities, which do not vary along the channel according to the auxiliary expression:

$$\dot{M} = \left[-\Lambda^*_{PP} + \frac{m_2 - m_1}{m(C_0)}(1 - C_0)\Lambda^*_{CP}\right]\frac{A'}{v(C_0)}\frac{P_{II} - P_I}{L}D_h. \tag{37}$$

Here, $\Lambda^*_{PP}$ and $\Lambda^*_{PC}$ are the average kinetic coefficients, which will be deduced such that Eq. 37 yields the correct mass flow rate. We note that the average kinetic coefficient has been earlier used for single gases (Sharipov and Seleznev 1998). Now, it is applied for mixtures with the assumption that the concentration is constant for the pressure-driven flow.

In order to achieve that the right-hand side of Eqs. 36 and 37 are equated to find

$$\Lambda_{PP}\frac{dP}{P_{II} - P_I} = \Lambda^*_{PP}dz\frac{D_h}{L} \tag{38}$$

$$\Lambda_{CP}\frac{dP}{P_{II} - P_I} = \Lambda^*_{CP}dz\frac{D_h}{L}. \tag{39}$$

Based on the definition of $\delta$, given in Eq. 8, it is easily deduced that $dP/(P_{II} - P_I) = d\delta/(\delta_{II} - \delta_I)$, where the rarefaction parameters $\delta_I$ and $\delta_{II}$ refer to pressures $P_I$ and $P_{II}$, respectively. Next, Eqs. 38 and 39 are integrated over $\delta$ in the interval $[\delta_I, \delta_{II}]$ and $0 \le z \le L/D_h$ to yield

$$\Lambda^*_{PP} = \frac{1}{\delta_{II} - \delta_I}\int_{\delta_I}^{\delta_{II}} \Lambda_{PP}d\delta, \tag{40}$$

$$\Lambda^*_{CP} = \frac{1}{\delta_{II} - \delta_I}\int_{\delta_I}^{\delta_{II}} \Lambda_{CP}d\delta. \tag{41}$$

The average kinetic coefficients can be calculated by Eqs. 40 and 41, provided that the kinetic coefficients for a specific gas mixture as a function of the rarefaction parameter along the channel have been estimated. Then, the mass flow rate is estimated from Eq. 37.

### 4.2 Concentration-driven flow

In this case, the flow is caused by a concentration drop between the two reservoirs. The concentrations in the upstream and downstream containers are given by $C_I$ and $C_{II}$, respectively, while the pressure and, therefore, the number density remain constant and equal to $P_0$ and $n_0$, respectively. The calculation is similar to the pressure-driven flow. Substituting Eqs. 14 and 15, with $X_P = 0$, into Eq. 13 the mass flow rate is given by

$$\dot{M} = \left[-\Lambda_{PC} + \frac{m_2 - m_1}{m(C)}(1 - C)\Lambda_{CC}\right]\frac{n_0 m(C)A'v(C)}{2C}\frac{dC}{dz}. \tag{42}$$

The mass flow rate is also defined in terms of reference quantities as

$$\dot{M} = \left[-\Lambda^*_{PC} + \frac{m_2 - m_1}{m(C_0)}(1 - C_0)\Lambda^*_{CC}\right] \times \frac{n_0 m(C_0)A'v(C_0)}{2C_0}\frac{C_{II} - C_I}{L}D_h. \tag{43}$$

Here, it is recalled that the pressure is considered constant for the present situation. As a consequence, the average kinetic coefficients can be applied. For the concentration-driven flow, since the concentration varies along the channel, the reference concentration $C_0$ is chosen as the average value between the two reservoirs, i.e., $C_0 = (C_I + C_{II})/2$. This also defines the reference mass $m(C_0)$ and characteristic velocity $v(C_0)$. Then, the right-hand sides of Eqs. 42 and 43 are equated to deduce

$$\Lambda_{PC}\frac{dC}{C_{II} - C_I}\frac{C_0}{C}\frac{m(C)v(C)}{m(C_0)v(C_0)} = \Lambda^*_{PC}dz\frac{D_h}{L}, \tag{44}$$

$$\Lambda_{CC}\frac{dC}{C_{II} - C_I}\frac{C_0}{C}\frac{1 - C}{1 - C_0}\frac{v}{v(C_0)} = \Lambda^*_{CC}dz\frac{D_h}{L}. \tag{45}$$

Integrating these equations along the channel, the average kinetic coefficients are obtained by

$$\Lambda^*_{PC} = \frac{1}{C_{II} - C_I}\int_{C_I}^{C_{II}} \frac{C_0}{C}\frac{m(C)v(C)}{m(C_0)v(C_0)}\Lambda_{PC}dC, \tag{46}$$

$$\Lambda^*_{CC} = \frac{1}{C_{II} - C_I}\int_{C_I}^{C_{II}} \frac{C_0}{C}\frac{1 - C}{1 - C_0}\frac{v(C)}{v(C_0)}\Lambda_{CC}dC. \tag{47}$$

Having calculated the average kinetic coefficients in terms of the concentration $C$ and the corresponding $\delta(C)$, the mass flow rate is obtained from Eq. 43 for the concentration-driven flow. In conclusion, we note that when the flow is driven by both pressure and concentration gradients, then the total mass flow rate is obtained by superimposing the two solutions.

## 5 Separation effect in rarefied binary gaseous flow

It is well known that in gas mixtures, consisting of various species, the particles of different types travel with different speeds. As the flow becomes more rarefied and the number of intermolecular collisions is reduced, this difference in the molecular velocities results to different macroscopic velocities for each species of the mixture as well. As a result, for gas mixtures flowing through long channels, the

concentration of the mixture may alter significantly in the flow direction. This phenomenon is known as the separation effect. It is observed in gaseous mixtures, but it is absent for single gases. The separation effect is very important in many applications including pumping, sampling, filtering, etc. (Sharipov and Kalempa 2005; Takata et al. 2007; Sugimoto 2009) and should be taken into consideration in the estimation of the mass flow rate.

A detailed investigation of the separation effect has been presented in Sharipov and Kalempa (2005) for binary gas flow through long tubes into vacuum, based on the prescribed number densities of the two reservoirs. Here, this procedure is slightly modified having as primitive variables, the pressure and concentration distributions. This treatment is equivalent to the one in Sharipov and Kalempa (2005), but it is considered as more straightforward and suitable for microflow applications, where, in general, the downstream pressure is not equal to zero, while the concentration of the gas in the downstream reservoir is known. The analysis, in addition to the exact estimation of the mass flow rate, provides in parallel the concentration and pressure variation along the channel.

The procedure is starting by introducing the mass flow rate of each component of the mixture, namely,

$$\dot{M}_\alpha = n_\alpha m_\alpha \int\int_{A'} u'_\alpha dx' dy', \tag{48}$$

with $\alpha = 1, 2$, while $\dot{M} = \dot{M}_1 + \dot{M}_2$. Our aim is to derive an expression for these fluxes as a function of the pressure and concentration gradients as driving terms. Utilizing Eq. 13, straightforward calculation shows that the component mass flow rates are connected to the fluxes $J_P$ and $J_C$ according to

$$\dot{M}_1 = -m_1(CJ_P + (1-C)J_C), \tag{49}$$

$$\dot{M}_2 = -m_2(1-C)(J_P - J_C). \tag{50}$$

At this point, we introduce the non-dimensional flow rates

$$J_\alpha = \frac{m(C_I)v(C_I)L}{m_\alpha P_I A' D_h}\dot{M}_\alpha, \tag{51}$$

where $\alpha = 1, 2$. The mass flow rates of each species, given by Eqs. 49 and 50, are introduced into Eq. 51 and then the fluxes $J_P$ and $J_C$, given by Eqs. 14 and 15, respectively, are substituted into the resulting equations to obtain

$$J_1 = -\frac{Pv(C)L}{P_I v(C_I)D_h}[(C\Lambda_{PP} + (1-C)\Lambda_{CP})X_P + (C\Lambda_{PC} + (1-C)\Lambda_{CC})X_C], \tag{52}$$

$$J_2 = -\frac{Pv(C)L}{P_I v(C_I)D_h}(1-C)[(\Lambda_{PP} - \Lambda_{CP})X_P + (\Lambda_{PC} - \Lambda_{CC})X_C]. \tag{53}$$

Utilizing the definitions of the characteristic velocity, the pressure and concentration gradients and the ideal gas law, Eqs. 52 and 53 are rewritten as

$$J_1 = -\frac{P}{P_I}\sqrt{\frac{m(C_I)}{m(C)}} \times \left[(C\Lambda_{PP} + (1-C)\Lambda_{CP})\frac{\partial P}{\partial \hat{z}}\frac{1}{P} + (C\Lambda_{PC} + (1-C)\Lambda_{CC})\frac{\partial C}{\partial \hat{z}}\frac{1}{C}\right], \tag{54}$$

$$J_2 = -\frac{P}{P_I}\sqrt{\frac{m(C_I)}{m(C)}}(1-C) \times \left[(\Lambda_{PP} - \Lambda_{CP})\frac{\partial P}{\partial \hat{z}}\frac{1}{P} + (\Lambda_{PC} - \Lambda_{CC})\frac{\partial C}{\partial \hat{z}}\frac{1}{C}\right], \tag{55}$$

where $0 \le \hat{z} \le 1$, defined as $\hat{z} = z'/L$, is the non-dimensional coordinate along the axis of the channel. The coupled ordinary differential Eqs. 54 and 55 are the main equations to be solved for the unknown distributions $P(\hat{z})$ and $C(\hat{z})$. These equations are supplemented by the following boundary conditions at the inlet and outlet of the micro-channel

$$P(0) = P_I, \quad P(1) = P_{II}, \tag{56}$$

$$C(0) = C_I, \quad C(1) = C_{II}. \tag{57}$$

It is mentioned that the reservoirs are considered large. As a consequence, the pressure and the concentrations are constant in the containers, and Eqs. 56 and 57 are well defined.

It is noted that the quantities $J_1$ and $J_2$ are unknown, and they will be deduced in an iterative manner such that the outlet boundary conditions at $\hat{z} = 1$ are satisfied. Initially some estimates of $J_1$ and $J_2$ are provided, and then the system of the ordinary differential equations is solved, starting from $\hat{z} = 0$ and moving up to $\hat{z} = 1$ , by applying a typical marching integration scheme, such as the Euler method. The computed values of the pressure and the concentration at the exit of the channel, $\hat{z} = 1$ , are compared to the corresponding boundary conditions. In order to find the values of $J_1$, $J_2$, a bisection root-finding method has been developed. Initially, two intervals are selected for $J_1$ and $J_2$. Then, the fluxes are determined in two joint iterations. The fluxes are always fixed at the middle values of the intervals. In each stage of the iteration, the corresponding interval is bisected, and the flux is reassigned to the new middle value. The changes of the fluxes in the algorithm are determined as follows. First, assuming the given value for the $J_2$ flux, $J_1$ is calculated depending on the concentration at the exit of the channel $C(1)$. If $C(1)$ is smaller (or larger) than $C_{II}$ then $J_1$ is decreased (or increased). In this way, $J_1$ is obtained, provided that the

concentration boundary condition is satisfied with a convergence criterion. After this procedure, the overall iteration starts with an updated value of $J_2$ depending on the pressure at the exit $P(1)$. If $P(1)$ is smaller (or larger) than $P_{II}$ then $J_2$ is decreased (or increased). The iteration on $J_2$ is repeated until the pressure boundary condition at the outlet is satisfied with a convergence criterion. Utilizing this method, $P(\hat{z})$ and $C(\hat{z})$ , as well as the quantities $J_1$ and $J_2$ are calculated. Finally, utilizing Eq. 51, the mass flow rates of each species and obviously of the gas mixture may be obtained.

In Sect. 6.2, based on the above methodology, results are presented for the mass flow rate for pressure-driven rarefied binary gas mixture flows through the triangular channel taking into account the separation effect. For this purpose, the normalized mass flow rate is introduced as

$$J_M = \frac{\nu(C_I)L}{P_I A' D_h}\dot{M}. \tag{58}$$

This quantity can be expressed in terms of $J_\alpha$, $\alpha = 1, 2$, by utilizing Eq. 51, in the more convenient form:

$$J_M = \frac{m_1}{m(C_I)}J_1 + \frac{m_2}{m(C_I)}J_2. \tag{59}$$

In addition to the estimation of $J_M$, the corresponding quantity without including the correction due to separation, is estimated. In order to achieve that and to be able to examine the importance of separation, it is necessary to introduce the quantities:

$$J_1^* = -[C\Lambda_{PP}^* + (1-C)\Lambda_{CP}^*]\frac{P_{II}-P_I}{P_I}, \tag{60}$$

$$J_2^* = -(1-C)[\Lambda_{PP}^* - \Lambda_{CP}^*]\frac{P_{II}-P_I}{P_I}, \tag{61}$$

The fluxes $J_\alpha^*$, $\alpha = 1, 2$ are based on the average kinetic coefficients, which are obtained from Eqs. 54 and 55 assuming zero concentration gradient ($X_C = 0$). Also, these fluxes correspond to $J_\alpha$, $\alpha = 1, 2$, obtained above including the separation effect. Finally, the normalized total mass flow on the basis of the average kinetic coefficients is given by

$$J_M^* = \frac{m_1}{m(C_I)}J_1^* + \frac{m_2}{m(C_I)}J_2^*. \tag{62}$$

We note that $J_M^*$ is the total mass flow rate without accounting for separation, and it corresponds to the mass flow rate given by Eq. 37 utilizing the normalization of Eq. 58.

## 6 Results

In this section, numerical results are presented in tabulated and graphical forms for the kinetic coefficients, the concentration and pressure variations along the channel, and the mass flow rates for certain flow configurations. In particular, the simulations include two binary mixtures, namely, the *Ne/Ar* mixture, with $m_1 = 20.183$ g/mol, $m_2 = 39.948$ g/mol and the *He/Xe* mixture, with $m_1 = 4.0026$ g/mol, $m_2 = 131.30$ g/mol, and the following three different cross sections: Two isosceles trapezoidal with $b/h = 0.5$ and 3, and one isosceles triangular ($b/h = 0$). In all these three cross sections, the angle $\omega = 54.74°$ (Fig. 1), which is the angle of micro-channels etched by KOH in silicon. In all the cases, purely diffuse accommodation is considered ($\sigma = 1$), while the collision frequencies in the kinetic equations are computed based on experimental data for the specific binary mixtures (Sharipov and Kalempa 2002; Naris et al. 2005).

### 6.1 Kinetic coefficients

The integro-differential system of equations, described in Sect. 3, is solved to obtain the kinetic coefficients. Depending upon the values of $\delta$ and the geometry, the discretization has been progressively refined to ensure grid-independent results up to several significant figures. The presented results have been obtained by utilizing the following discretization: In the molecular velocity space, the number of discrete velocities is set to $M \times N = 16 \times 300$ for $\delta < 1$ and $M \times N = 16 \times 72$ for $\delta \geq 1$. Here, $M$ and $N$ denote the number of magnitudes and polar angles of the discrete velocity vector, respectively. In the physical space, for the triangular cross section, the number of nodes along its base is set equal to 1000 for $\delta \leq 1$ and to 1400 for $\delta > 1$, while for the trapezoidal cross section, the number of nodes along its large base $B$ is set equal to 1500 for all values of $\delta$. The iteration process is terminated when the absolute difference between subsequent values of the dimensionless flow rates is less than $10^{-6}$.

Tables 1, 2, and 3 depict the kinetic coefficients $\Lambda_{PP}$, $\Lambda_{CP}$, and $\Lambda_{CC}$ for the whole range of $C$ and for a very wide range of $0 \leq \delta \leq 100$. As mentioned before $\Lambda_{CP} = \Lambda_{PC}$. With regard to $\Lambda_{PP}$, it can be deduced that it has a minimum in the transient region for all the cases. This corresponds to the so-called Knudsen-minimum phenomenon, that is, the total flow rate has a minimum in the transition region. The Knudsen-minimum appears for pressure-driven gas flows through channels or between plates in the transient region. It can be observed in both single component gases and gaseous mixtures. Considering $\Lambda_{CP}$, which is a cross effect and corresponds to a diffusion flux due to a pressure gradient, it can be seen that it increases as the rarefaction parameter $\delta$ is decreased. This demonstrates that the velocity difference between the components of the binary mixture, which causes the diffusion flux, becomes larger as the flow becomes more

**Table 1** Kinetic coefficients for the isosceles triangular channel ($\omega = 54.74°$)

| $\delta$ | $C$ | Ne/Ar | | | He/Xe | | |
|---|---|---|---|---|---|---|---|
| | | $\Lambda_{PP}$ | $\Lambda_{CP}$ | $\Lambda_{CC}$ | $\Lambda_{PP}$ | $\Lambda_{CP}$ | $\Lambda_{CC}$ |
| 0 | 0.0 | 0.934 | 0.000 | 0.000 | 0.934 | 0.000 | 0.000 |
| 0.1 | 0.0 | 0.878 | 0.000 | 0.000 | 0.878 | 0.000 | 0.000 |
| 0.5 | 0.0 | 0.839 | 0.000 | 0.000 | 0.839 | 0.000 | 0.000 |
| 1 | 0.0 | 0.844 | 0.000 | 0.000 | 0.844 | 0.000 | 0.000 |
| 5 | 0.0 | 0.107(+1) | 0.000 | 0.000 | 0.107(+1) | 0.000 | 0.000 |
| 10 | 0.0 | 0.142(+1) | 0.000 | 0.000 | 0.142(+1) | 0.000 | 0.000 |
| 50 | 0.0 | 0.438(+1) | 0.000 | 0.000 | 0.438(+1) | 0.000 | 0.000 |
| 100 | 0.0 | 0.813(+1) | 0.000 | 0.000 | 0.813(+1) | 0.000 | 0.000 |
| 0 | 0.2 | 0.959 | 0.722(−1) | 0.294 | 0.163(+1) | 0.793 | 0.100(+1) |
| 0.1 | 0.2 | 0.901 | 0.660(−1) | 0.263 | 0.153(+1) | 0.732 | 0.922 |
| 0.5 | 0.2 | 0.859 | 0.526(−1) | 0.209 | 0.139(+1) | 0.615 | 0.775 |
| 1 | 0.2 | 0.860 | 0.427(−1) | 0.173 | 0.132(+1) | 0.528 | 0.667 |
| 5 | 0.2 | 0.108(+1) | 0.165(−1) | 0.735(−1) | 0.133(+1) | 0.258 | 0.331 |
| 10 | 0.2 | 0.143(+1) | 0.900(−2) | 0.424(−1) | 0.160(+1) | 0.155 | 0.202 |
| 50 | 0.2 | 0.439(+1) | 0.188(−2) | 0.956(−2) | 0.446(+1) | 0.364(−1) | 0.482(−1) |
| 100 | 0.2 | 0.813(+1) | 0.943(−3) | 0.486(−2) | 0.819(+1) | 0.185(−1) | 0.246(−1) |
| 0 | 0.5 | 0.975 | 0.165 | 0.975 | 0.225(+1) | 0.158(+1) | 0.225(+1) |
| 0.1 | 0.5 | 0.916 | 0.150 | 0.865 | 0.211(+1) | 0.147(+1) | 0.208(+1) |
| 0.5 | 0.5 | 0.871 | 0.118 | 0.679 | 0.190(+1) | 0.124(+1) | 0.176(+1) |
| 1 | 0.5 | 0.871 | 0.946(−1) | 0.554 | 0.178(+1) | 0.107(+1) | 0.152(+1) |
| 5 | 0.5 | 0.109(+1) | 0.353(−1) | 0.228 | 0.161(+1) | 0.541 | 0.779 |
| 10 | 0.5 | 0.144(+1) | 0.191(−1) | 0.130 | 0.181(+1) | 0.329 | 0.480 |
| 50 | 0.5 | 0.439(+1) | 0.399(−2) | 0.290(−1) | 0.458(+1) | 0.779(−1) | 0.116 |
| 100 | 0.5 | 0.814(+1) | 0.201(−2) | 0.147(−1) | 0.830(+1) | 0.397(−1) | 0.592(−1) |
| 0 | 0.8 | 0.962 | 0.236 | 0.314(+1) | 0.212(+1) | 0.167(+1) | 0.344(+1) |
| 0.1 | 0.8 | 0.904 | 0.213 | 0.275(+1) | 0.199(+1) | 0.155(+1) | 0.317(+1) |
| 0.5 | 0.8 | 0.861 | 0.165 | 0.212(+1) | 0.182(+1) | 0.132(+1) | 0.270(+1) |
| 1 | 0.8 | 0.862 | 0.131 | 0.171(+1) | 0.173(+1) | 0.116(+1) | 0.236(+1) |
| 5 | 0.8 | 0.109(+1) | 0.470(−1) | 0.675 | 0.166(+1) | 0.619 | 0.126(+1) |
| 10 | 0.8 | 0.143(+1) | 0.253(−1) | 0.380 | 0.188(+1) | 0.386 | 0.787 |
| 50 | 0.8 | 0.439(+1) | 0.528(−2) | 0.839(−1) | 0.468(+1) | 0.935(−1) | 0.192 |
| 100 | 0.8 | 0.814(+1) | 0.266(−2) | 0.425(−1) | 0.840(+1) | 0.479(−1) | 0.985(−1) |
| 0 | 1.0 | 0.934 | 0.270 | | 0.934 | 0.771 | |
| 0.1 | 1.0 | 0.878 | 0.242 | | 0.878 | 0.701 | |
| 0.5 | 1.0 | 0.839 | 0.185 | | 0.839 | 0.600 | |
| 1 | 1.0 | 0.844 | 0.145 | | 0.844 | 0.533 | |
| 5 | 1.0 | 0.107(+1) | 0.508(−1) | | 0.107(+1) | 0.306 | |
| 10 | 1.0 | 0.142(+1) | 0.272(−1) | | 0.142(+1) | 0.199 | |
| 50 | 1.0 | 0.438(+1) | 0.570(−2) | | 0.438(+1) | 0.512(−1) | |
| 100 | 1.0 | 0.813(+1) | 0.287(−2) | | 0.813(+1) | 0.265(−1) | |

rarefied. The results of $\Lambda_{CP}$ for $C = 1$ may be considered as limiting values corresponding to a concentration very close but not equal to one. For $C = 1$, the gas is one-component, and diffusion flux does not appear. However, for the limiting case $C \to 1$, the diffusion flux and $\Lambda_{CP}$ are finite. The $\Lambda_{CP}$ limiting value is presented in the table. In regard to $\Lambda_{CC}$, it is seen that it increases with decreasing rarefaction parameter. Hence, the direct diffusion effects are stronger in a rarefied

**Table 2** Kinetic coefficients for the isosceles trapezoidal channel ($\omega = 54.74°$, $b/h = 0.5$)

| $\delta$ | $C$ | Ne/Ar | | | He/Xe | | |
|---|---|---|---|---|---|---|---|
| | | $\Lambda_{PP}$ | $\Lambda_{CP}$ | $\Lambda_{CC}$ | $\Lambda_{PP}$ | $\Lambda_{CP}$ | $\Lambda_{CC}$ |
| 0 | 0.0 | 0.904 | 0.000 | 0.000 | 0.904 | 0.000 | 0.000 |
| 0.1 | 0.0 | 0.852 | 0.000 | 0.000 | 0.852 | 0.000 | 0.000 |
| 0.5 | 0.0 | 0.816 | 0.000 | 0.000 | 0.816 | 0.000 | 0.000 |
| 1 | 0.0 | 0.821 | 0.000 | 0.000 | 0.821 | 0.000 | 0.000 |
| 5 | 0.0 | 0.104(+1) | 0.000 | 0.000 | 0.104(+1) | 0.000 | 0.000 |
| 10 | 0.0 | 0.138(+1) | 0.000 | 0.000 | 0.138(+1) | 0.000 | 0.000 |
| 50 | 0.0 | 0.427(+1) | 0.000 | 0.000 | 0.427(+1) | 0.000 | 0.000 |
| 100 | 0.0 | 0.792(+1) | 0.000 | 0.000 | 0.792(+1) | 0.000 | 0.000 |
| 0 | 0.2 | 0.928 | 0.699(−1) | 0.284 | 0.158(+1) | 0.768 | 0.971 |
| 0.1 | 0.2 | 0.874 | 0.640(−1) | 0.256 | 0.148(+1) | 0.711 | 0.896 |
| 0.5 | 0.2 | 0.835 | 0.514(−1) | 0.205 | 0.135(+1) | 0.600 | 0.756 |
| 1 | 0.2 | 0.837 | 0.419(−1) | 0.170 | 0.129(+1) | 0.517 | 0.653 |
| 5 | 0.2 | 0.105(+1) | 0.164(−1) | 0.733(−1) | 0.130(+1) | 0.256 | 0.329 |
| 10 | 0.2 | 0.139(+1) | 0.895(−2) | 0.423(−1) | 0.156(+1) | 0.155 | 0.201 |
| 50 | 0.2 | 0.428(+1) | 0.188(−2) | 0.956(−2) | 0.435(+1) | 0.364(−1) | 0.482(−1) |
| 100 | 0.2 | 0.793(+1) | 0.942(−3) | 0.486(−2) | 0.799(+1) | 0.185(−1) | 0.246(−1) |
| 0 | 0.5 | 0.944 | 0.160 | 0.944 | 0.218(+1) | 0.153(+1) | 0.218(+1) |
| 0.1 | 0.5 | 0.889 | 0.145 | 0.841 | 0.205(+1) | 0.142(+1) | 0.202(+1) |
| 0.5 | 0.5 | 0.847 | 0.115 | 0.665 | 0.185(+1) | 0.121(+1) | 0.171(+1) |
| 1 | 0.5 | 0.847 | 0.929(−1) | 0.545 | 0.174(+1) | 0.105(+1) | 0.149(+1) |
| 5 | 0.5 | 0.106(+1) | 0.351(−1) | 0.227 | 0.158(+1) | 0.537 | 0.774 |
| 10 | 0.5 | 0.140(+1) | 0.190(−1) | 0.130 | 0.176(+1) | 0.328 | 0.479 |
| 50 | 0.5 | 0.428(+1) | 0.399(−2) | 0.290(−1) | 0.447(+1) | 0.778(−1) | 0.116 |
| 100 | 0.5 | 0.793(+1) | 0.200(−2) | 0.147(−1) | 0.809(+1) | 0.397(−1) | 0.592(−1) |
| 0 | 0.8 | 0.932 | 0.229 | 0.304(+1) | 0.205(+1) | 0.162(+1) | 0.333(+1) |
| 0.1 | 0.8 | 0.877 | 0.207 | 0.268(+1) | 0.193(+1) | 0.150(+1) | 0.308(+1) |
| 0.5 | 0.8 | 0.837 | 0.161 | 0.208(+1) | 0.177(+1) | 0.129(+1) | 0.263(+1) |
| 1 | 0.8 | 0.839 | 0.128 | 0.168(+1) | 0.169(+1) | 0.114(+1) | 0.232(+1) |
| 5 | 0.8 | 0.106(+1) | 0.467(−1) | 0.673 | 0.162(+1) | 0.615 | 0.125(+1) |
| 10 | 0.8 | 0.139(+1) | 0.252(−1) | 0.380 | 0.184(+1) | 0.385 | 0.785 |
| 50 | 0.8 | 0.428(+1) | 0.528(−2) | 0.839(−1) | 0.456(+1) | 0.935(−1) | 0.192 |
| 100 | 0.8 | 0.793(+1) | 0.265(−2) | 0.425(−1) | 0.819(+1) | 0.479(−1) | 0.985(−1) |
| 0 | 1.0 | 0.904 | 0.262 | | 0.904 | 0.746 | |
| 0.1 | 1.0 | 0.852 | 0.235 | | 0.852 | 0.681 | |
| 0.5 | 1.0 | 0.816 | 0.181 | | 0.816 | 0.586 | |
| 1 | 1.0 | 0.821 | 0.143 | | 0.821 | 0.522 | |
| 5 | 1.0 | 0.104(+1) | 0.505(−1) | | 0.104(+1) | 0.305 | |
| 10 | 1.0 | 0.138(+1) | 0.271(−1) | | 0.138(+1) | 0.199 | |
| 50 | 1.0 | 0.427(+1) | 0.569(−2) | | 0.427(+1) | 0.512(−1) | |
| 100 | 1.0 | 0.792(+1) | 0.287(−2) | | 0.792(+1) | 0.265(−1) | |

gas rather than in a dense gas. The variation of the kinetic coefficients in terms of $C$ is more significant in the case of the *He/Xe* mixture compared to the corresponding one for the *Ne/Ar* mixture. As expected, the qualitative behavior of the findings are in agreement with the one obtained in previous studies (Sharipov and Kalempa 2002; Naris et al. 2005) for

**Table 3** Kinetic coefficients for the isosceles trapezoidal channel ($\omega = 54.74°$, $b/h = 3$)

| $\delta$ | $C$ | Ne/Ar | | | He/Xe | | |
|---|---|---|---|---|---|---|---|
| | | $\Lambda_{PP}$ | $\Lambda_{CP}$ | $\Lambda_{CC}$ | $\Lambda_{PP}$ | $\Lambda_{PC}$ | $\Lambda_{CC}$ |
| 0 | 0.0 | 0.965 | 0.000 | 0.000 | 0.965 | 0.000 | 0.000 |
| 0.1 | 0.0 | 0.892 | 0.000 | 0.000 | 0.892 | 0.000 | 0.000 |
| 0.5 | 0.0 | 0.830 | 0.000 | 0.000 | 0.830 | 0.000 | 0.000 |
| 1 | 0.0 | 0.818 | 0.000 | 0.000 | 0.818 | 0.000 | 0.000 |
| 5 | 0.0 | 0.965 | 0.000 | 0.000 | 0.965 | 0.000 | 0.000 |
| 10 | 0.0 | 0.123(+1) | 0.000 | 0.000 | 0.123(+1) | 0.000 | 0.000 |
| 50 | 0.0 | 0.354(+1) | 0.000 | 0.000 | 0.354(+1) | 0.000 | 0.000 |
| 100 | 0.0 | 0.649(+1) | 0.000 | 0.000 | 0.649(+1) | 0.000 | 0.000 |
| 0 | 0.2 | 0.991 | 0.746(−1) | 0.304 | 0.169(+1) | 0.819 | 0.104(+1) |
| 0.1 | 0.2 | 0.916 | 0.675(−1) | 0.267 | 0.156(+1) | 0.748 | 0.941 |
| 0.5 | 0.2 | 0.850 | 0.530(−1) | 0.208 | 0.139(+1) | 0.617 | 0.775 |
| 1 | 0.2 | 0.834 | 0.427(−1) | 0.170 | 0.130(+1) | 0.524 | 0.659 |
| 5 | 0.2 | 0.975 | 0.166(−1) | 0.727(−1) | 0.122(+1) | 0.254 | 0.325 |
| 10 | 0.2 | 0.124(+1) | 0.905(−2) | 0.422(−1) | 0.140(+1) | 0.155 | 0.200 |
| 50 | 0.2 | 0.355(+1) | 0.188(−2) | 0.956(−2) | 0.362(+1) | 0.364(−1) | 0.482(−1) |
| 100 | 0.2 | 0.649(+1) | 0.944(−3) | 0.486(−2) | 0.655(+1) | 0.185(−1) | 0.246(−1) |
| 0 | 0.5 | 0.101(+1) | 0.170 | 0.101(+1) | 0.233(+1) | 0.164(+1) | 0.233(+1) |
| 0.1 | 0.5 | 0.932 | 0.153 | 0.879 | 0.216(+1) | 0.150(+1) | 0.212(+1) |
| 0.5 | 0.5 | 0.863 | 0.119 | 0.674 | 0.190(+1) | 0.124(+1) | 0.176(+1) |
| 1 | 0.5 | 0.845 | 0.947(−1) | 0.544 | 0.175(+1) | 0.107(+1) | 0.151(+1) |
| 5 | 0.5 | 0.982 | 0.355(−1) | 0.226 | 0.150(+1) | 0.533 | 0.765 |
| 10 | 0.5 | 0.124(+1) | 0.192(−1) | 0.130 | 0.161(+1) | 0.327 | 0.476 |
| 50 | 0.5 | 0.356(+1) | 0.399(−2) | 0.290(−1) | 0.374(+1) | 0.778(−1) | 0.116 |
| 100 | 0.5 | 0.650(+1) | 0.201(−2) | 0.147(−1) | 0.665(+1) | 0.398(−1) | 0.592(−1) |
| 0 | 0.8 | 0.995 | 0.244 | 0.325(+1) | 0.219(+1) | 0.173(+1) | 0.356(+1) |
| 0.1 | 0.8 | 0.919 | 0.217 | 0.279(+1) | 0.203(+1) | 0.158(+1) | 0.323(+1) |
| 0.5 | 0.8 | 0.852 | 0.166 | 0.210(+1) | 0.182(+1) | 0.132(+1) | 0.269(+1) |
| 1 | 0.8 | 0.837 | 0.131 | 0.168(+1) | 0.170(+1) | 0.115(+1) | 0.233(+1) |
| 5 | 0.8 | 0.978 | 0.472(−1) | 0.669 | 0.154(+1) | 0.607 | 0.123(+1) |
| 10 | 0.8 | 0.124(+1) | 0.254(−1) | 0.379 | 0.168(+1) | 0.382 | 0.780 |
| 50 | 0.8 | 0.355(+1) | 0.528(−2) | 0.839(−1) | 0.383(+1) | 0.935(−1) | 0.192 |
| 100 | 0.8 | 0.650(+1) | 0.266(−2) | 0.425(−1) | 0.674(+1) | 0.479(−1) | 0.985(−1) |
| 0 | 1.0 | 0.965 | 0.279 | | 0.965 | 0.797 | |
| 0.1 | 1.0 | 0.892 | 0.246 | | 0.892 | 0.712 | |
| 0.5 | 1.0 | 0.830 | 0.185 | | 0.830 | 0.593 | |
| 1 | 1.0 | 0.818 | 0.145 | | 0.818 | 0.519 | |
| 5 | 1.0 | 0.965 | 0.510(−1) | | 0.965 | 0.296 | |
| 10 | 1.0 | 0.123(+1) | 0.273(−1) | | 0.123(+1) | 0.195 | |
| 50 | 1.0 | 0.354(+1) | 0.570(−2) | | 0.354(+1) | 0.512(−1) | |
| 100 | 1.0 | 0.649(+1) | 0.287(−2) | | 0.649(+1) | 0.265(−1) | |

binary flow through circular and rectangular channels. Of course, there are significant quantitative differences.

The geometric effects on the kinetic coefficients are also investigated by comparing the corresponding results for trapezoid and rectangular channels (Naris et al. 2005). For the comparison, we have selected isosceles trapezoidal and rectangular channels with the same height and the same hydrodynamic diameter. The flow problem is characterized

**Table 4** Geometric effects on the kinetic coefficients, *He/Xe* mixture with $C = 0.5$. The results are denoted by T and R for trapezoidal and rectangular channels, respectively

| $h/w$ | $\delta^h$ | $\Lambda_{PP}$ | | $\Lambda_{CP}$ | | $\Lambda_{CC}$ | |
|---|---|---|---|---|---|---|---|
| | | T | R | T | R | T | R |
| 1 | 0 | 0.219(+1) | 0.203(+1) | 0.154(+1) | 0.142(+1) | 0.219(+1) | 0.202(+1) |
| 1 | 1 | 0.174(+1) | 0.165(+1) | 0.105(+1) | 0.101(+1) | 0.149(+1) | 0.143(+1) |
| 1 | 10 | 0.177(+1) | 0.170(+1) | 0.329 | 0.327 | 0.479 | 0.477 |
| 0.5 | 0 | 0.224(+1) | 0.209(+1) | 0.157(+1) | 0.147(+1) | 0.224(+1) | 0.209(+1) |
| 0.5 | 1 | 0.169(+1) | 0.162(+1) | 0.975 | 0.943 | 0.138(+1) | 0.134(+1) |
| 0.5 | 10 | 0.185(+1) | 0.180(+1) | 0.260 | 0.259 | 0.380 | 0.379 |
| 0.1 | 0 | 0.278(+1) | 0.264(+1) | 0.196(+1) | 0.186(+1) | 0.278(+1) | 0.264(+1) |
| 0.1 | 1 | 0.160(+1) | 0.159(+1) | 0.879 | 0.873 | 0.124(+1) | 0.123(+1) |
| 0.1 | 10 | 0.172(+1) | 0.172(+1) | 0.198 | 0.198 | 0.290 | 0.291 |

by the height to width ratio $h/w$ of the rectangular channel and the rarefaction parameter $\delta^h$ corresponding to the height (Naris et al. 2005). Note that the corresponding rarefaction parameter in the present approach is $\delta = (D_h/h)\ \delta^h$. In addition, the kinetic coefficients, $\Lambda_{ij}^h$ appearing in Naris et al. (2005) needs to be converted to our formulation as $\Lambda_{ij} = (h/D_h)\Lambda_{ij}^h$ . In Table 4, $\Lambda_{ij}$ is presented as a function of $h/w$ and $\delta^h$ for the *He/Xe* mixture with concentration $C = 0.5$. It can be seen that the difference between the kinetic coefficients for the trapezoid and the rectangular channels becomes smaller as $h/w$ decreases. This demonstrates that the trapezoid and rectangular channels provide the same results in the limiting case as $h/w$ tends to zero and the two cross sections become identical.

In addition to the above comparison, the flow of a selected gaseous mixture (He/Xe, with $C = 0.5$) has been also simulated in a square channel by the same method of this study. That geometry can be recovered by an orthogonal triangle $\omega = 45°$ and specular boundary condition at the bottom wall. The results have been compared to the available data in the literature (Naris et al. 2005). We have found an excellent agreement between the two situations in a wide range of the rarefaction.

The present results in terms of the kinetic coefficients refer to the whole range of the rarefaction and concentration. However, it is interesting to compare the results to the slip flow results for a single gas presented by Morini et al (2004). The comparison is based on the Poiseuille number $Po = fRe$, which is the Fanning friction factor times the Reynolds number. In this case, the Poiseuille number is given by $Po = \delta/\Lambda_{PP}$ for $C = 0$ (or $C = 1$). For describing the rarefaction, Morini et al. utilized a modified Knudsen number, $Kn_v$, which includes the first-order slip coefficient. It is related to the rarefaction parameter such that $Kn_v = \alpha_s/\delta$, where $\alpha_s = 1.018$ is the slip coefficient of the S kinetic model. Note that the McCormack model reduces to the S kinetic model for a single gas. In Table 5, we present the kinetic and the slip flow results for triangular and trapezoidal channels in terms of $Kn_v$. It is clearly visible that the kinetic result converges to the slip solution when $Kn_v \to 0$. This is the case for both the triangular and trapezoid channels.

**Table 5** The Poiseuille number for triangular and trapezoid channels as a function of $Kn_v$ for a single gas ($C = 0$). The symbols K and S stand for the kinetic and slip solutions, respectively

| $Kn_v$ | $Po$ | | | |
|---|---|---|---|---|
| | $b/h = 0$ | | $b/h = 2$ | |
| | K | S | K | S |
| 0.100 | 0.710(+1) | 0.748(+1) | 0.784(+1) | 0.828(+1) |
| 0.075 | 0.809(+1) | 0.838(+1) | 0.902(+1) | 0.937(+1) |
| 0.050 | 0.936(+1) | 0.954(+1) | 0.106(+2) | 0.108(+2) |
| 0.025 | 0.110(+2) | 0.111(+2) | 0.127(+2) | 0.127(+2) |
| 0.010 | 0.123(+2) | 0.123(+2) | 0.143(+2) | 0.143(+2) |

### 6.2 Pressure-driven binary gas flow in long microchannels

The methodology described in Sect. 5 is implemented to obtain the exact mass flow rate accounting for the gas separation and the estimated value on the basis of the average kinetic coefficients for certain binary gas flows through channels. In addition, the concentration and pressure distributions along the channel are computed. Results are presented for the *He/Xe* gas mixture flowing through the isosceles triangular channel. The coupled ordinary differential Eqs. 54 and 55 are numerically integrated, along $0 \le \hat{z} \le 1$ , with a first-order scheme having $\Delta\hat{z} = 1/500$ for several sets of boundary conditions. The iteration process for estimating $J_1$ and $J_2$ is terminated when an

absolute convergence criterion of $10^{-5}$ on both $C(1)$ and $P(1)$ is satisfied.

In Fig. 2, the concentration distribution $C(\hat{z})$ along the channel is shown for pressure ratio $\Pi = P_I/P_{II} = 3$ and 6, and for $\delta_I = 1$ and 10, with $C_I = C_{II} = 0.5$. The corresponding results for $C_I = C_{II} = 0.8$ are presented in Fig. 3. The chosen values of the pressure ratio and the rarefaction parameter are typical in microflow experiments and applications. Since in both cases $C_I = C_{II}$, the flow is purely due to a sustainable pressure difference between the inlet and outlet of the channel. It is clearly seen that in all the cases, the concentration along the channel is not constant. As the gas mixture is flowing through the channel, due to the separation phenomenon, the concentration of the light species starting from $C_I$ is decreasing along the larger part of the channel, from $\hat{z} = 0$ up to about $\hat{z} = 0.8$ and then it starts increasing to reach the imposed boundary value of $C_{II}$ at $\hat{z} = 1$. Also, in both figures, when $\Pi = 3$ the variation of $C(\hat{z})$ from the constant values of the two reservoirs is very small, while when $\Pi = 6$ the corresponding deviation becomes significant. This is a clear indication that as the pressure ratio is increased, gas separation is intensified. In addition, it appears that for the same pressure ratio, the concentration drop is larger at $\delta_I = 10$ compared to $\delta_I = 1$. A similar behavior of the variation of $C(\hat{z})$ in terms $\delta$ has been also observed by Sharipov and Kalempa

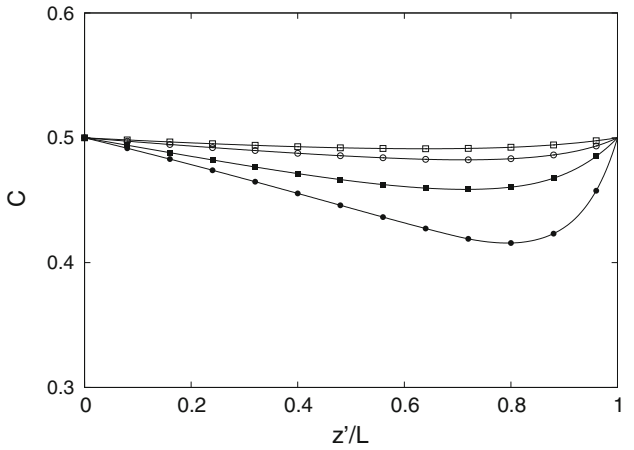


**Fig. 2** Concentration distribution along the isosceles triangular channel for the *He*/*Xe* mixture, with $C_I = C_{II} = 0.5$. Symbols *open square*, *open circle* represent results for $\delta_I = 1$ and 10, respectively, with pressure ratio $\Pi = 3$, while *filled square*, *filled circle* represent the corresponding results, with pressure ratio $\Pi = 6$

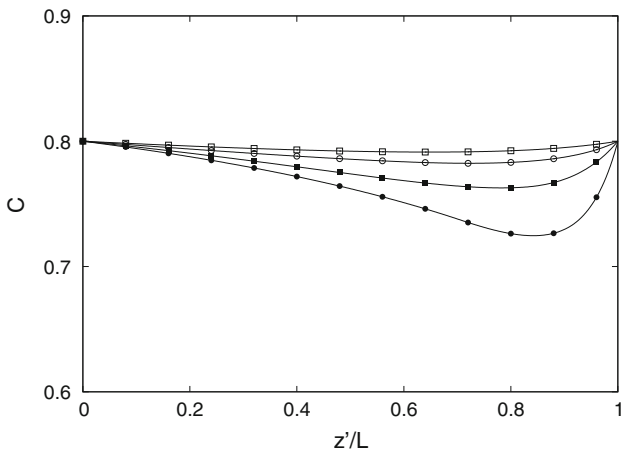


**Fig. 3** Concentration distribution along the isosceles triangular channel for the *He*/*Xe* mixture, with $C_I = C_{II} = 0.8$. Symbols *open square*, *open circle* represent results for $\delta_I = 1$ and 10, respectively, with pressure ratio $\Pi = 3$, while *filled square*, *filled circle* represent the corresponding results, with pressure ratio $\Pi = 6$

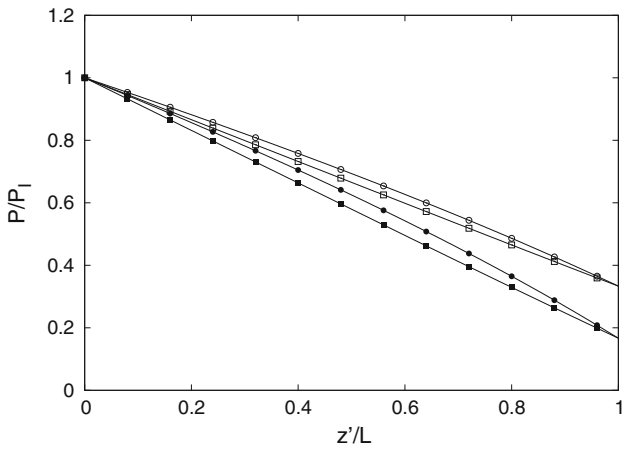


**Fig. 4** Pressure distribution along the isosceles triangular channel for the *He*/*Xe* mixture, with $C_I = C_{II} = 0.5$. Symbols *open square*, *open circle* represent results for $\delta_I = 1$ and 10, respectively, with pressure ratio $\Pi = 3$, while *filled square*, *filled circle* represent the corresponding results, with pressure ratio $\Pi = 6$

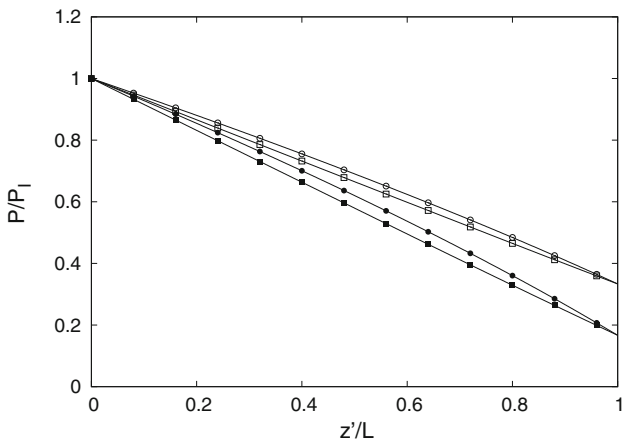


**Fig. 5** Pressure distribution along the isosceles triangular channel for the *He*/*Xe* mixture, with $C_I = C_{II} = 0.8$. Symbols *open square*, *open circle* represent results for $\delta_I = 1$ and 10, respectively, with pressure ratio $\Pi = 3$, while *filled square*, *filled circle* represent the corresponding results, with pressure ratio $\Pi = 6$

(2005). The pressure distributions along the channel are presented in Figs. 4 and 5, corresponding to the cases shown in Figs. 2 and 3, respectively. In both figures, the effect of the rarefaction parameter is clearly observed. At higher values of the rarefaction parameter, the pressure distribution becomes increasingly nonlinear. This nonlinear behaviour vanishes as the gas becomes more dilute.

In Tables 6 and 7, the fluxes and the normalized mass flow rates with and without gas separation are tabulated for $C_I = C_{II} = 0.5$ and $C_I = C_{II} = 0.8$, respectively. The values of the pressure ratios are $\Pi = 5$ and 10, while of the rarefaction parameters are $\delta_I = 0.1$, 1, 5, 10, and 30. It is seen that for $\delta_I = 0.1$ and 1, the differences between $J_M$ and $J_M^*$ are negligible. In this range of rarefaction, the effect of the separation phenomenon is not important and may be ignored. However, for $\delta_I = 5$, 10, and 30, there are some discrepancies. It is seen that in the case of the large pressure ratio, the relative error defined as $\Delta = (J_M - J_M^*)/J_M$ varies between 3.7–7.6% for $\delta_I = 5$, 6.0–9.8% for $\delta_I = 10$, and 5.4–6.2% for $\delta_I = 30$. It is interesting to note that the separation effect becomes more important in the limit between the transition and slip regimes, i.e., in moderate and not in highly rarefied atmospheres. However, the phenomenon is characterized by the inlet rarefaction parameter, $\delta_I$. Since the average rarefaction parameter is smaller in the channel than at the inlet, the separation effect is the strongest in the transition region. The reason of this is that both rarefaction effects and intermolecular collisions are important in regard to the separation. Concerning the mass flow rates, the discrepancies between $J_M$ and $J_M^*$ are always larger for $\Pi = 10$ compared to the corresponding ones for $\Pi = 5$. Overall, the largest deviation is about 10% and occurs for $C_I = C_{II} = 0.5$, $\Pi = 10$ and $\delta_I = 10$.

Finally, note that that the gas separation occurs in mixtures as a result of the component-dependent collision mechanism between the gas molecules. The separation has no primary connection to the wall accommodation. The gas separation occurs for pure diffuse walls, as has been shown in this analysis. Non-diffuse walls have minor impact on the separation effect. The role of the accommodation coefficient can be important in comparative studies against experiments. In fact, the accommodation coefficient

**Table 6** Normalized fluxes and mass flow rates with and without separation effects (*He/Xe*, $C_I = C_{II} = 0.5$)

| $\Pi$ | $\delta_I$ | $J_1$ | $J_2$ | $J_1^*$ | $J_2^*$ | $J_M$ | $J_M^*$ | $\Delta$(%) |
|---|---|---|---|---|---|---|---|---|
| 5 | 0.1 | 0.147(+1) | 0.263 | 0.147(+1) | 0.263 | 0.597 | 0.597 | 0.0 |
| | 1 | 0.124(+1) | 0.271 | 0.125(+1) | 0.270 | 0.599 | 0.597 | 0.3 |
| | 5 | 0.905 | 0.370 | 0.961 | 0.357 | 0.772 | 0.750 | 2.8 |
| | 10 | 0.801 | 0.485 | 0.883 | 0.460 | 0.989 | 0.944 | 4.5 |
| | 30 | 0.966 | 0.876 | 0.104(+1) | 0.835 | 0.176(+1) | 0.168(+1) | 4.4 |
| 10 | 0.1 | 0.166(+1) | 0.296 | 0.166(+1) | 0.296 | 0.673 | 0.673 | 0.0 |
| | 1 | 0.141(+1) | 0.304 | 0.142(+1) | 0.302 | 0.673 | 0.671 | 0.4 |
| | 5 | 0.103(+1) | 0.411 | 0.111(+1) | 0.391 | 0.857 | 0.826 | 3.7 |
| | 10 | 0.891 | 0.535 | 0.102(+1) | 0.497 | 0.109(+1) | 0.103(+1) | 6.0 |
| | 30 | 0.104(+1) | 0.942 | 0.115(+1) | 0.886 | 0.189(+1) | 0.179(+1) | 5.4 |

**Table 7** Normalized fluxes and mass flow rates with and without separation effects (*He/Xe*, $C_I = C_{II} = 0.8$)

| $\Pi$ | $\delta_I$ | $J_1$ | $J_2$ | $J_1^*$ | $J_2^*$ | $J_M$ | $J_M^*$ | $\Delta$(%) |
|---|---|---|---|---|---|---|---|---|
| 5 | 0.1 | 0.156(+1) | 0.708(−1) | 0.156(+1) | 0.708(−1) | 0.528 | 0.528 | 0.0 |
| | 1 | 0.136(+1) | 0.833(−1) | 0.137(+1) | 0.821(−1) | 0.556 | 0.552 | 0.7 |
| | 5 | 0.113(+1) | 0.144 | 0.120(+1) | 0.131 | 0.794 | 0.747 | 5.8 |
| | 10 | 0.112(+1) | 0.200 | 0.120(+1) | 0.180 | 0.105(+1) | 0.965 | 7.6 |
| | 30 | 0.154(+1) | 0.362 | 0.160(+1) | 0.340 | 0.182(+1) | 0.173(+1) | 4.9 |
| 10 | 0.1 | 0.176(+1) | 0.797(−1) | 0.176(+1) | 0.797(−1) | 0.594 | 0.594 | 0.0 |
| | 1 | 0.154(+1) | 0.929(−1) | 0.156(+1) | 0.911(−1) | 0.623 | 0.618 | 0.9 |
| | 5 | 0.127(+1) | 0.160 | 0.137(+1) | 0.142 | 0.885 | 0.818 | 7.6 |
| | 10 | 0.124(+1) | 0.222 | 0.136(+1) | 0.193 | 0.116(+1) | 0.104(+1) | 9.8 |
| | 30 | 0.166(+1) | 0.390 | 0.175(+1) | 0.360 | 0.196(+1) | 0.184(+1) | 6.2 |

depends on the gas and the channel surface and may not be equal to unity (Ewart et al. 2007; Graur et al. 2009; Maurer et al. 2003). In such cases, the accommodation coefficient can be adjusted in the theory and the method.

The present method for calculating the flow rate can be used in practical applications. The advantageous nature of the method is that it is based on the kinetic description of the flow and properly takes into account the diffusion effects. The kinetic problem is solved locally with modest computational effort. In comparison, solving kinetic problems by the DSMC method is computationally more demanding for low speed flows which is the case in micro-gas flow applications.

## 7 Concluding remarks

The flow of binary gaseous mixtures through channels with triangular and trapezoidal cross section, due to pressure and concentration gradients, has been investigated in the whole range of the Knudsen number. The flow is modeled by the McCormack kinetic model subject to diffuse-specular boundary conditions. The system of linear integro-differential equations has been solved by discretizing in the physical space using a finite difference scheme on a boundary fitted triangular lattice, and in the molecular velocity space by an upgraded version of the discrete velocity method. The kinetic coefficients have been calculated for *Ne/Ar* and *He/Xe* mixtures. In addition, a detailed methodology has been presented for converting the dimensionless kinetic results to mass flow rates by taking into account the variation of the concentration of the mixture as it is flowing through the channel due to the well-known gas separation effect. Results are presented for isosceles triangular and trapezoidal channels with an acute angle of 54.74°, which are very common in microfluidics applications. For the examined flow configurations, the discrepancies between the estimated total mass flow rate with and without taking into account gas separation may be up to about 10%. The presented analysis and results may be useful in the design of micro-systems and for accurate comparison with corresponding experimental study.

**Acknowledgments** This research obtained financial support from the European Community's Seventh Framework programme (FP7/2007-2013) under grant agreement no 215504. The views and opinions expressed herein do not necessarily reflect those of the European Commission.

## Appendix 1: elements of the McCormack model

The McCormack collision term reads such that

$$\begin{aligned} L_{\alpha\beta}h_\alpha &= -\gamma_{\alpha\beta}h_\alpha \\ &+ 2\sqrt{\frac{m_\alpha}{m}}\left[\gamma_{\alpha\beta}u_\alpha - \nu^{(1)}_{\alpha\beta}(u_\alpha - u_\beta) - \frac{1}{2}\nu^{(2)}_{\alpha\beta}\left(q_\alpha - \frac{m_\alpha}{m_\beta}q_\beta\right)\right]c_{\alpha z} \\ &+ 4[(\gamma_{\alpha\beta} - \nu^{(3)}_{\alpha\beta})p_{\alpha xz} + \nu^{(4)}_{\alpha\beta}p_{\beta xz}]c_{\alpha z}c_{\alpha x} \\ &+ 4[(\gamma_{\alpha\beta} - \nu^{(3)}_{\alpha\beta})p_{\alpha yz} + \nu^{(4)}_{\alpha\beta}p_{\beta yz}]c_{\alpha z}c_{\alpha y} \\ &+ \frac{4}{5}\sqrt{\frac{m_\alpha}{m}}\left[(\gamma_{\alpha\beta} - \nu^{(5)}_{\alpha\beta})q_\alpha + \nu^{(6)}_{\alpha\beta}\sqrt{\frac{m_\beta}{m_\alpha}}q_\beta - \frac{5}{4}\nu^{(2)}_{\alpha\beta}(u_\alpha - u_\beta)\right] \\ &\times c_{\alpha z}\left(c^2_\alpha - \frac{5}{2}\right). \end{aligned} \tag{63}$$

The collision frequencies in the McCormack model are defined as follows:

$$\nu^{(1)}_{\alpha\beta} = \frac{16m_{\alpha,\beta}}{3\ m_\alpha}n_\beta\Omega^{11}_{\alpha\beta}, \tag{64}$$

$$\nu^{(2)}_{\alpha\beta} = \frac{64}{15}\left(\frac{m_{\alpha,\beta}}{m_\alpha}\right)^2 n_\beta\left(\Omega^{12}_{\alpha\beta} - \frac{5}{2}\Omega^{11}_{\alpha\beta}\right), \tag{65}$$

$$\nu^{(3)}_{\alpha\beta} = \frac{16}{5}\left(\frac{m_{\alpha,\beta}}{m_\alpha}\right)^2\frac{m_\alpha}{m_\beta}n_\beta\left(\frac{10}{3}\Omega^{11}_{\alpha\beta} + \frac{m_\beta}{m_\alpha}\Omega^{22}_{\alpha\beta}\right), \tag{66}$$

$$\nu^{(4)}_{\alpha\beta} = \frac{16}{5}\left(\frac{m_{\alpha,\beta}}{m_\alpha}\right)^2\frac{m_\alpha}{m_\beta}n_\beta\left(\frac{10}{3}\Omega^{11}_{\alpha\beta} - \Omega^{22}_{\alpha\beta}\right), \tag{67}$$

$$\nu^{(5)}_{\alpha\beta} = \frac{64}{15}\left(\frac{m_{\alpha,\beta}}{m_\alpha}\right)^2\frac{m_\alpha}{m_\beta}n_\beta\Gamma^{(5)}_{\alpha\beta}, \tag{68}$$

$$\nu^{(6)}_{\alpha\beta} = \frac{64}{15}\left(\frac{m_{\alpha,\beta}}{m_\alpha}\right)^2\left(\frac{m_\alpha}{m_\beta}\right)^{3/2}n_\beta\Gamma^{(6)}_{\alpha\beta}, \tag{69}$$

where

$$\begin{aligned} \Gamma^{(5)}_{\alpha\beta} &= \Omega^{22}_{\alpha\beta} + \left(\frac{15m_\alpha}{4m_\beta} + \frac{25m_\beta}{8m_\alpha}\right)\Omega^{11}_{\alpha\beta} \\ &\quad - \left(\frac{m_\beta}{2m_\alpha}\right)\left(5\Omega^{12}_{\alpha\beta} - \Omega^{13}_{\alpha\beta}\right), \end{aligned} \tag{70}$$

$$\Gamma^{(6)}_{\alpha\beta} = -\Omega^{22}_{\alpha\beta} + \frac{55}{8}\Omega^{11}_{\alpha\beta} - \frac{5}{2}\Omega^{12}_{\alpha\beta} + \frac{1}{2}\Omega^{13}_{\alpha\beta}. \tag{71}$$

In addition,

$$m_{\alpha,\beta} = \frac{m_\alpha m_\beta}{m_\alpha + m_\beta}. \tag{72}$$

In the above expressions, $\Omega^{11}_{\alpha\beta}, \Omega^{12}_{\alpha\beta}, \Omega^{13}_{\alpha\beta}, \Omega^{22}_{\alpha\beta}$ are the Chapman–Cowling integrals (Sharipov and Kalempa 2002; Naris et al. 2005). The $\gamma_{\alpha\ \beta}$ collision frequencies appear in the combination $\gamma_\alpha = \gamma_{\alpha\alpha} + \gamma_{\alpha\beta}$ defined by

$$\gamma_\alpha = \frac{S_\alpha S_\beta - \nu^{(4)}_{\alpha\beta}\nu^{(4)}_{\beta\alpha}}{S_\beta + \nu^{(4)}_{\alpha\beta}} \tag{73}$$

with $S_\alpha = \nu^{(3)}_{\alpha\alpha} - \nu^{(4)}_{\alpha\alpha} + \nu^{(3)}_{\alpha\beta}$. In the expressions of $\gamma_\alpha$, $S_\alpha$ and Eq. 73, $\alpha, \beta = [1, 2]$ and $\alpha \neq \beta$. The $\omega_\alpha$ coefficient is given by

$$\omega_\alpha = \sqrt{\frac{m_\alpha}{m}}\left[\frac{C}{\gamma_1} + \frac{1-C}{\gamma_2}\right]\delta. \tag{74}$$

## Appendix 2: The upgraded discrete velocity method

Diffusion synthetic accelerated discrete velocity algorithms have been applied in a series of flows simulated on rectangular grids (Naris et al. 2004). Here, this methodology is accordingly adapted in triangular lattices. The accelerated scheme is derived by operating according to the McCormack kinetic equations.

First, the following Hermite moments

$$U^\alpha_{mn} = \frac{1}{\pi}\int_{-\infty}^{\infty}\int_{-\infty}^{\infty} H_m(c_{\alpha x})H_n(c_{\alpha y})\Phi_\alpha e^{-c^2_{\alpha x}-c^2_{\alpha y}}dc_{\alpha x}dc_{\alpha y}, \tag{75}$$

$$Q^\alpha_{mn} = \frac{1}{\pi}\int_{-\infty}^{\infty}\int_{-\infty}^{\infty} H_m(c_{\alpha x})H_n(c_{\alpha y}) \left[\Psi_\alpha + \left(c^2_{\alpha x} + c^2_{\alpha y} - \frac{5}{2}\right)\Phi_\alpha\right] e^{-c^2_{\alpha x}-c^2_{\alpha y}}dc_{\alpha x}dc_{\alpha y}. \tag{76}$$

are introduced. Here, $U^\alpha_{00}$ and $Q^\alpha_{00}$ are the velocity and the heat flow vectors, respectively, for component $\alpha = 1, 2$. In the following, we use the $m + n \le 2$ moment-system.

Then, by taking the zeroth- and first-order Hermitian moment of Eqs. 23 and 24 and manipulating the resulting equations, the following system of four diffusion equations is obtained:

$$\frac{\partial^2 U^\alpha_{00}}{\partial x^2} + \frac{\partial^2 U^\alpha_{00}}{\partial y^2} - 2\omega^2_\alpha(v^{(3)}_{\alpha\alpha} + v^{(3)}_{\alpha\beta} - v^{(4)}_{\alpha\alpha})F_{\alpha\beta} + 2\omega_\alpha\omega_\beta\sqrt{\frac{m_\beta}{m_\alpha}}v^{(4)}_{\alpha\beta}G_{\alpha\beta} = -\frac{1}{2}\frac{\partial^2 U^\alpha_{20}}{\partial x^2} - \frac{1}{2}\frac{\partial^2 U^\alpha_{02}}{\partial y^2} - \frac{\partial^2 U^\alpha_{11}}{\partial x\partial y} + \omega_\alpha\sqrt{\frac{m}{m_\alpha}}[(S_\alpha - v^{(4)}_{\alpha\beta})X_P + (S_\alpha\eta_\alpha - v^{(4)}_{\alpha\beta}\eta_\beta)X_C] \tag{77}$$

$$\frac{\partial^2 Q^\alpha_{00}}{\partial x^2} + \frac{\partial^2 Q^\alpha_{00}}{\partial y^2} + 2\omega^2_\alpha\left[-(v^{(5)}_{\alpha\alpha} + v^{(5)}_{\alpha\beta} - v^{(6)}_{\alpha\alpha})Q^\alpha_{00} + \sqrt{\frac{m_\beta}{m_\alpha}}v^{(6)}_{\alpha\beta}Q^\beta_{00} - \frac{5}{4}v^{(2)}_{\alpha\beta}(U^\alpha_{00} - U^\beta_{00})\right] + 2\omega^2_\alpha(\gamma_\alpha - v^{(3)}_{\alpha\alpha} - v^{(3)}_{\alpha\beta} + v^{(4)}_{\alpha\alpha})F_{\alpha\beta} + 2\omega_\alpha\omega_\beta\sqrt{\frac{m_\beta}{m_\alpha}}v^{(4)}_{\alpha\beta}G_{\alpha\beta} = -\frac{1}{2}\frac{\partial^2 U^\alpha_{20}}{\partial x^2} - \frac{1}{2}\frac{\partial^2 U^\alpha_{02}}{\partial y^2} - \frac{\partial^2 U^\alpha_{11}}{\partial x\partial y} - \omega_\alpha\sqrt{\frac{m}{m_\alpha}}\left[\left(\gamma_\alpha - S_\alpha + v^{(4)}_{\alpha\beta}\right)X_P + (\gamma_\alpha\eta_\alpha - S_\alpha\eta_\alpha + v^{(4)}_{\alpha\beta}\eta_\beta)X_C\right], \tag{78}$$

where

$$F_{\alpha\beta} = v^{(1)}_{\alpha\beta}(U^\alpha_{00} - U^\beta_{00}) + \frac{v^{(2)}_{\alpha\beta}}{2}\left(Q^\alpha_{00} - \frac{m_\alpha}{m_\beta}Q^\beta_{00}\right), \tag{79}$$

$$G_{\alpha\beta} = v^{(1)}_{\alpha\beta}(U^\beta_{00} - U^\alpha_{00}) + \frac{v^{(2)}_{\alpha\beta}}{2}\left(Q^\beta_{00} - \frac{m_\beta}{m_\alpha}Q^\alpha_{00}\right) \tag{80}$$

with $\alpha, \beta = [1, 2]$ and $\alpha \neq \beta$.

Equations 77 and 78 are discretized in the physical space on the same triangular grid as the kinetic Eqs. 23 and 24. The spatial derivatives are calculated via a second-order finite-difference scheme obtained from the Taylor's expansion of the moments around the nodes of the grid. The solution of the diffusion equation proceeds in parallel with the iterative solution of the kinetic equations, Eqs. 23 and 24. In each iteration stage, the kinetic equations are solved for the unknown distribution functions. On the basis of the distribution functions, the higher moments in Eqs. 77 and 78 with $m + n = 2$ are calculated by the integral expressions (75) and (76). Then, these higher moments, $U^\alpha_{20}, U^\alpha_{02}, U^\alpha_{11}$ and $Q^\alpha_{20}, Q^\alpha_{02}, Q^\alpha_{11}$ , are substituted into the right-hand sides of Eqs. 77 and 78. These latter equations, Eqs. 77 and 78, are solved for the unknown velocity and heat flow vector $U^\alpha_{00}$ and $Q^\alpha_{00}$ . The solution of the diffusion equation is performed via a successive-over-relaxation solver. Finally, the accelerated moments, $U^\alpha_{00}$ and $Q^\alpha_{00}$, are substituted into the right-hand sides of Eqs. 23 and 24. Then, these kinetic equations are solved for the distribution functions in the next iteration stage.

## References


Aoki K (2001) 39th AIAA aerospace science meeting and exhibit. Reno, 2001–0874

Bird GA (1994) Molecular gas dynamics and the direct simulation of gas flows. Oxford University Press, Oxford

Breyiannis G, Varoutis S, Valougeorgis D (2008) Rarefied gas flow in concentric annular tube: estimation of the Poiseuille number and the exact hydraulic diameter. Eur J Mech B/Fluids 27(5):609–622

Cercignani C (1988) The Boltzmann equation and its application. Springer, New York

Colin S (2005) Rarefaction and compressibility effects on steady and transient gas flows in microchannels. Microfluid Nanofluidics 1(3):268–279

Colin S, Lalonde P et al (2004) Validation of a second-order slip flow model in rectangular microchannels. Heat Transf Eng 25(3):23–30

Ewart T, Perrier P, Graur IA, Meolans JG (2007) Mass flow rate measurements in a microchannel from hydrodynamic to near free molecular regimes. J Fluid Mech 584:337–356

Ferziger JH, Kaper HG (1972) Mathematical theory of transport processes in gases. North Holland, Amstderdam

Graur I, Sharipov F (2007) Gas flow through an elliptical tube over the whole range of the gas rarefaction. Eur J Mech B/Fluids 27:335–345

Graur I, Sharipov F (2008) Non-isothermal flow of rarefied gas through a long pipe with elliptic cross section. Microfluid Nanofluidics 6:267–275

Graur IA, Perrier P, Ghozlani W, Molans JG (2009) Measurements of tangential momentum accommodation coefficient for various gases in plane microchannel. Phys Fluids 21:102004

Ho CM, Tai YC (1998) Micro-electro-mechanical systems (MEMS) and fluid flows. Ann Rev Fluid Mech 30:579–612

Kandlikar SG, Garimella S et al (2006) Heat transfer and fluid flow in minichannels and microchannels. Elsevier, Oxford

Karniadakis GE, Beskok A (2002) Micro flows. Springer, New York

Li D (ed) (2008) Encyclopedia of microfluidics and nanofluidics. Springer, New York

Lockerby DA, Reese JM (2008) On the modelling of isothermal gas flows at the microscale. J Fluid Mech 604:235–261

Maurer J, Tabeling P, Joseph P, Willaime H (2003) Second-order slip laws in microchannels for helium and nitrogen. Phys Fluids 15:2613–2621

McCormack FJ (1973) Construction of linearized kinetic models for gaseous mixtures and molecular gases. Phys Fluids 16(12):2095–2105

Morini GL, Spiga M, Tartarini P (2004) The rarefaction effect on the friction factor of gas flow in microchannels. Superlattice Microst 35:587–599

Morini GL, Lorenzini M, Spiga M (2005) A criterion for experimental validation of slip-flow models for incompressible rarefied gases through microchannels. Microfluid Nanofluidics 1:190–196

Naris S, Valougeorgis D (2008) Rarefied gas flow in a triangular duct based on a boundary fitted lattice. Eur J Mech B/Fluids 27:810–822

Naris S, Valougeorgis D, Sharipov F, Kalempa D (2004) Discrete velocity modelling of gaseous mixture flows in MEMS. Superlattice Microst 35(3–6):629–643

Naris S, Valougeorgis D, Sharipov F, Kalempa D (2005) Flow of gaseous mixtures through rectangular microchannels driven by pressure, temperature and concentration gradients. Phys Fluids 17(10):100607.1–100607.12

Pitakarrnop J, Geoffroy S, Colin S, Baldas L (2008) Slip flow in triangular and trapezoidal microchannels. Int J Heat Technol 26(1):167–174

Pitakarnnop J, Varoutis S, Valougeorgis D, Geoffroy S, Baldas L, Colin S (2010) A novel experimental setup for gas microflows. Microfluid Nanofluidics 8:57–72

Sharipov F (1994) Onsager-Casimir reciprocity relations for open gaseous systems at arbitrary rarefaction. III. Theory and its application for gaseous mixtures. Phys A 209:457–476

Sharipov F (1999) Rarefied gas flow through a long rectangular channel. J Vac Sci Technol A 17:3062

Sharipov F, Kalempa D (2002) Gaseous mixture flow through a long tube at arbitrary Knudsen number. J Vac Sci Technol A 20(3):814–822

Sharipov F, Kalempa D (2005) Separation phenomena for gaseous mixture flowing through a long tube into vacuum. Phys Fluids 17:127102.1–8

Sharipov F, Seleznev V (1998) Data on internal rarefied gas flows. J Phys Chem Ref Data 27:657–706

Sharipov F, Cumin LMG, Kalempa D (2004) Plane Couette flow of binary gaseous mixture in the whole range of the Knudsen number. Eur J Mech B/Fluids 23:899–906

Sharipov F, Cumin LMG, Kalempa D (2007) Heat flux through a binary gaseous mixture over the whole range of the Knudsen number. Phys A 378:183–193

Siewert CE, Valougeorgis D (2004a) Concise and accurate solutions to half-space binary-gas flow problems defined by the McCormack model and specular-diffuse wall conditions. Eur J Mech B/Fluids 23:709–726

Siewert CE, Valougeorgis D (2004b) The McCormack model: channel flow of a binary gas mixture driven by temperature, pressure and density gradients. Eur J Mech B/Fluids 23:645–664

Sugimoto H (2009) Experiment on the gas separation effect of the pump driven by the thermal edge flow. Rarefied gas dynamics: 26th international symposium, AIP 978-0-7354-0615-5/09

Szalmas L (2007) Multiple-relaxation time lattice Boltzmann method for the finite Knudsen number region. Phys A 379(2):401–408

Takata S, Sugimoto H, Kosuge S (2007) Gas separation by means of the Knudsen compressor. Eur J Mech B/Fluids 26:155–181

Varoutis S, Naris S, Hauer V, Day C, Valougeorgis D (2009) Experimental and computational investigation of gas flows through long channels of various cross sections in the whole range of the Knudsen number. J Vac Sci Technol A 27(1):89–100